SILICON-GERMANIUM BICMOS DEVICE AND CIRCUIT DESIGN FOR EXTREME ENVIRONMENT APPLICATIONS

A Thesis
Presented to
The Academic Faculty

by

Ryan M. Diestelhorst

In Partial Fulfillment
of the Requirements for the Degree
Master of Science in the
School of Electrical and Computer Engineering

Georgia Institute of Technology
May 2009

SILICON-GERMANIUM BICMOS DEVICE AND CIRCUIT DESIGN FOR EXTREME ENVIRONMENT APPLICATIONS

Approved By:

Professor John D. Cressler, Advisor
School of Electrical and Computer Engineering
Georgia Institute of Technology

Professor John Papapolymerou
School of Electrical and Computer Engineering
Georgia Institute of Technology

Professor Stephen E. Ralph
School of Electrical and Computer Engineering
Georgia Institute of Technology

Date Approved: April 2nd, 2009

ACKNOWLEDGEMENTS

I would like to thank my endlessly supportive parents for their unwavering belief in my capabilities and positive influence on my direction. I would like to thank my brother, my step-mother, and my entire extended family for making the idea of “home” have weight and meaning in my life. Without them I would be without foundation. Finally, I would like to thank John Cressler for shaping my education and giving me the opportunities that have fostered my development as a scientist and engineer.

TABLE OF CONTENTS

LIST OF TABLES

LIST OF FIGURES

SUMMARY

Silicon-germanium (SiGe) BiCMOS technology platforms have proven invaluable for implementing a wide variety of digital, RF, and mixed-signal applications in extreme environments such as space, where maintaining high levels of performance in the presence of low temperatures and background radiation is paramount. This work will focus on the investigation of the total-dose radiation tolerance of a third generation complementary SiGe:C BiCMOS technology platform. Tolerance will be quantified under proton and X-ray radiation sources for both the *npn* and *pnp* HBT, as well as for an operational amplifier built with these devices. Furthermore, a technique known as junction isolation radiation hardening will be proposed and tested with the goal of improving the SEE sensitivity of the *npn* in this platform by reducing the charge collected by the subcollector in the event of a direct ion strike. To the author's knowledge, this work presents the first design and measurement results for this form of RHBD.

CHAPTER I

INTRODUCTION

1.1 Motivation

Silicon-germanium (SiGe) BiCMOS technology continues to receive significant interest as a candidate for extreme environment electronics applications, and is particularly well-suited for operation in the cryogenic temperature and radiation-rich conditions typically found in space exploration. Cost considerations force customers in this niche market to look to technologies with a high potential for integration while placing very stringent constraints on their ability to operate reliably for long periods of time under harsh conditions. Within such constraints SiGe has been demonstrated to excel [1]. The fabrication steps required to build a self-aligned SiGe HBT are compatible with the low-cost CMOS processes that have historically dominated the market, allowing analog and RF systems to be easily integrated with the digital electronics required to control them. In addition, the SiGe HBT has been shown to be extremely resilient to total dose effects induced by the ionizing radiation that permeates the space environment [2], [3], [4].

Temperature also represents a very important design constraint in extreme environments. On the lunar surface, for example, temperatures can range from -180˚C in the shade to 120˚C in the sun. Typical systems designed to operate in this environment must be housed in "warm boxes," which serve to mitigate the temperature swings affecting vital electronics at the cost of substantial power consumption and bulk. The SiGe HBT has the potential to eliminate the need for such equipment as its performance

is governed by minority carrier physics that improve as temperature decreases. This is in stark contrast to the Si HBT, whose performance metrics degrade substantially with temperature. The difference can be attributed directly to the effects of the bandgap engineered base, which conveniently arrange the thermal energy component, kT, such that improvements in β, f_T, and V_A are seen as temperature decreases. These low-temperature effects are intrinsic to the SiGe HBT without additional temperature hardening, and can be leveraged to build circuits that are operational across extremely wide temperature ranges with minimal effort [5].

An exciting recent development in the realm of SiGe technology has been the production of high-performance complementary (*npn* + *pnp*) SiGe technologies, enabling a host of new complementary circuit techniques to be employed in analog / mixed-signal and RF design. Complementary bipolar technologies possess a number of advantages over their *npn*-only counterparts, including: the ability to significantly reduce the power consumption of high-performance analog circuits; providing more efficient active loads and voltage / current sources; and enabling the use of high-speed push-pull drivers [6]. Historically, however, it has been no simple matter to incorporate the process steps required for *pnp* SiGe HBT fabrication into an optimized *npn* SiGe HBT process without compromising its performance [4].

Despite these numerous advantages, however, commercially-available, bulk SiGe HBTs are especially prone to single event effects (SEE). These arise when a high-energy ion collides with the silicon near the device. Electron-hole pairs are produced in great numbers along the track of the ion through the substrate, which, when collected by the device, can produce voltage transients substantial enough to corrupt data. Previous

studies have shown unhardened SiGe Gb/s digital logic to have high saturated cross sections and low upset thresholds by virtue of the charge collection dynamics within the lightly-doped substrate [7]. In many high-performance SiGe technology platforms some degree of substrate isolation is achieved through the use of 8 μm deep trench isolation (DTI) which surrounds the subcollector. While the DTI does serve to insulate the subcollector from ion deposited charge outside of the DTI boundaries, it also confines those same charges when an ion strikes the device within the DTI boundary.

One particularly simple form of device-level radiation hardening by design (RHBD) intended to improve this effect consists of an n-type implant surrounding the DTI. By applying a positive DC bias to the "n-ring" external to the DTI, it can effectively shunt charge away from the sensitive collector node for outside DTI strikes [8]. The main limitation of this RHBD technique has proven to be the DTI itself, however, due to the fact that an emitter-center strike (worst case for SEU) leaves the majority of free electrons in a location where the n-ring cannot collect them. The present work investigates the effects of using a new junction isolation hardening scheme on the charge collection dynamics of a third-generation, high-performance SiGe BiCMOS technology that does not employ deep trench isolation. As will be shown, this junction isolation RHBD approach is easy to implement, and is more effective for SEU mitigation than any other device-level RHBD approach demonstrated to date.

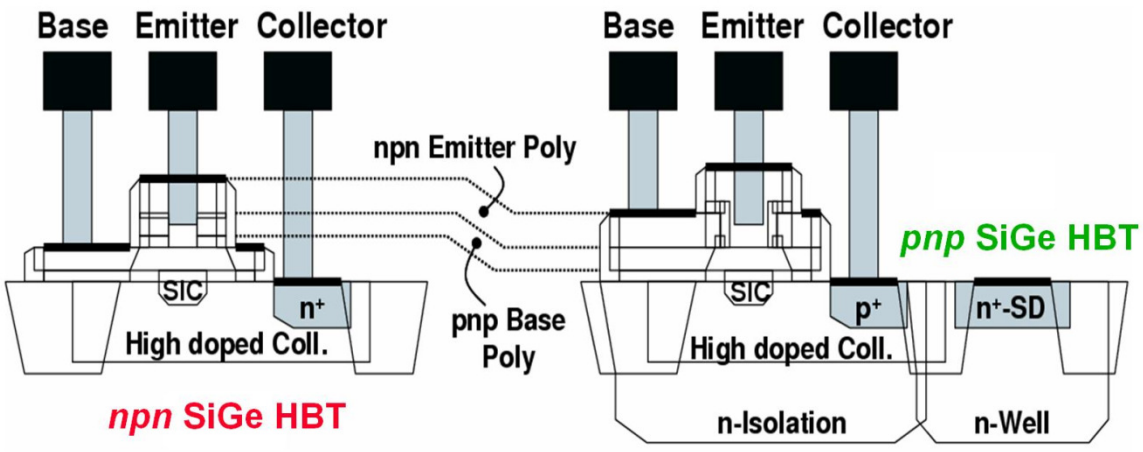

Figure 1: Cross sectional diagram of the 3rd generation 200 GHz / 90 GHz *npn* and *pnp* structure.

1.2 SiGe BiCMOS Technology Overview

The complementary SiGe:C HBT technology (Figure 1) under investigation was developed by IHP, and integrates isolated *pnp* SiGe HBTs with f_T / f_{max} values of 90 GHz / 125 GHz into a core 0.25 µm 200 GHz / 200 GHz *npn* SiGe BiCMOS platform [9]. The performance of the carbon-doped *npn* SiGe HBTs, which are built using a novel collector design without deep trench isolation, is not significantly affected by the additional *pnp* fabrication steps. Furthermore, the performance of the *pnp* SiGe HBTs is enhanced by reducing phosphorous diffusion via carbon doping, as is commonly practiced in *npn* SiGe HBTs. The uniquely designed subcollector of the *npn* SiGe HBT is fully contained within the sidewalls of the STI, thereby reducing the collector-substrate junction area and eliminating deep trench isolation entirely, reducing cost dramatically [10]. The low complexity, 10-mask process also takes advantage of the use of a single active area without isolation between the active emitter and collector contact regions, thereby lowering collector resistance and decreasing capacitive coupling to the substrate [9].

CHAPTER II

TOTAL DOSE CHARACTERIZATION

2.1 Test Conditions and Facilities

X-ray irradiation was performed at Vanderbilt University using an ARACOR model 4100 10-keV X-ray source, at a dose rate of 0.54 krad(SiO_2)/s. In addition, 63-MeV proton irradiation was performed at the Crocker Nuclear Laboratory, University of California at Davis, at a dose rate of 1.05 krad(SiO_2)/s. The proton dosimetry measurements, which are accurate to about 10%, used a 5-foil secondary emission monitor calibrated against a Faraday cup. The radiation source exhibited beam spatial uniformity of roughly 15% over a 2.0 cm radius circular area [11]. The data presented here were collected over a six month period including two separate experiments on multiple samples at each facility [4].

In both cases the SiGe HBTs were wire-bonded into 28-pin DIP packages for biasing purposes and were measured at room temperature in incremental dose steps. Both grounded and forward-active ($I_C \approx 1$ mA, $V_{CB} = 0$ V) bias conditions were used during irradiation on devices with varying emitter geometry. The forward-active bias condition was tested to more closely emulate the effects of total dose radiation on an operating circuit in space. AC devices were subject to X-ray exposure under a passive bias condition (floating), with S-parameter measurements taken before exposure and after returning from the facility at Vanderbilt [4].

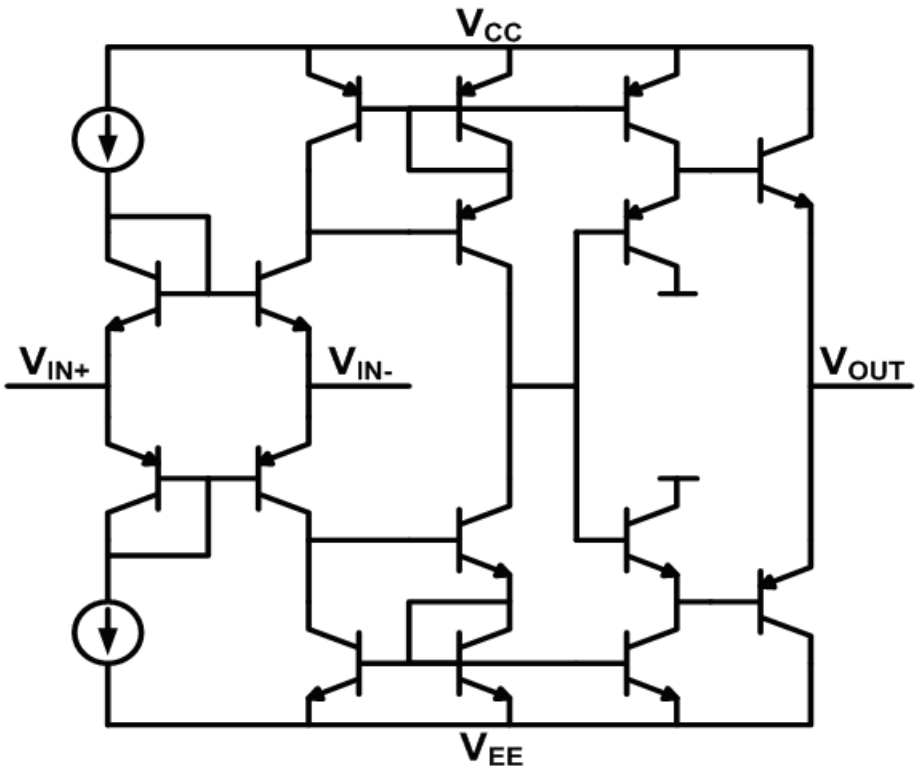

Figure 2: Schematic of the current feedback operational amplifier utilizing only *npn* and *pnp* HBTs.

2.2 Current Feedback Operational Amplifier

A current-feedback operational amplifier utilizing only *npn* and *pnp* SiGe HBTs in the investigated technology is shown in Figure 2, with various figures-of-merit under normal operation summarized in Table 1. This type of amplifier offers a high slew rate while its design conveniently decouples gain from bandwidth [12]. The diode-connected SiGe HBTs followed by the emitter-follower stage act as a voltage buffer between the non-inverting and inverting inputs. Wilson current mirrors are used to convert the input current differential into a high-impedance voltage output and a push-pull voltage buffer enables the amplifier to drive low-impedance loads [13], [14], [4].

Table 1: Current Feedback Operational Amplifier Characteristics

Power Supply	+/- 2.5 V
Designed Bias Current	1 mA
Quiescent Power	54 mW
Transresistance	20.6 kΩ
Unity Gain Bandwidth	200 MHz
Positive Slew Rate (C_L = 51 pF)	+ 414 V/μs
Negative Slew Rate (C_L = 51 pF)	- 327 V/ μs

The amplifier was irradiated with all terminals grounded to a total X-ray dose of 1.8 Mrad(SiO_2). For measurement and biasing purposes, the circuit was mounted and wire-bonded on a custom-made printed circuit board containing resistive feedback networks, supply decoupling capacitors, and SMA launchers for the input and output signals. Measurements were made both before and after irradiation at three distinct bias conditions, including: unity gain with 1.0 mA input tail current, finite gain with 100 μA tail current, and finite gain with 10 μA tail current [4].

2.3 Total Dose Radiation Results

Figures 3 and 4 depict the forward and inverse mode Gummel characteristics for both *npn* and *pnp* (A_E=0.42x0.84 μm^2) devices with increasing X-ray and proton dose, respectively. The bias condition during exposure had little impact on total incurred damage, and as such these and all subsequent results are shown for the forward-active case only. The characteristic increase in base current density with increasing ionizing radiation dose has been previously documented and is caused by the production of generation-recombination (G/R) centers near the emitter-base (EB) spacer [15]. Also previously documented in a different, lower-performance C-SiGe technology is the

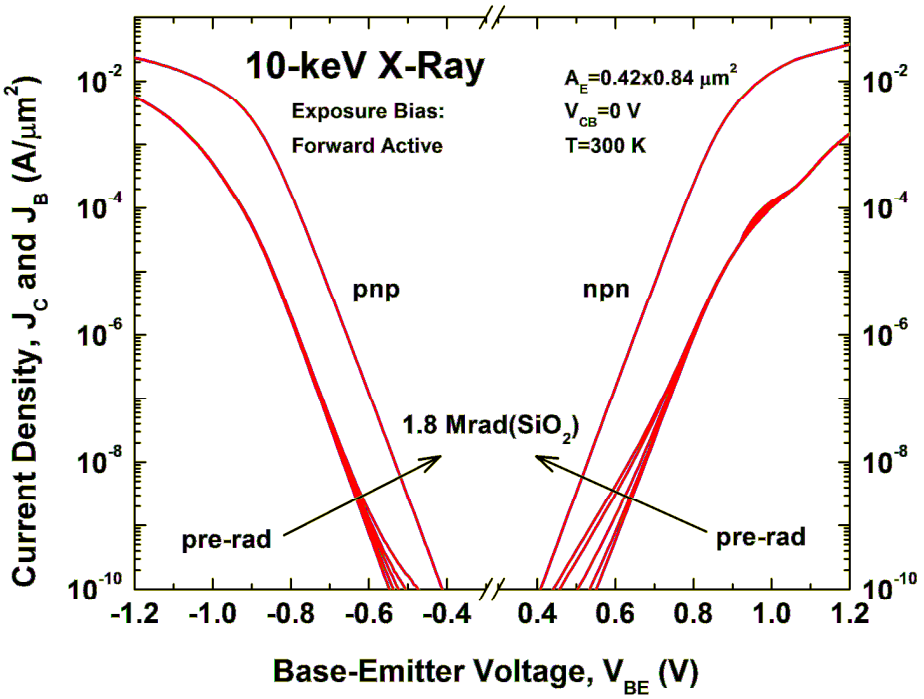

Figure 3: Forward mode *npn* and *pnp* Gummel characteristics from forward-active 10-keV X-ray exposure up to 1.8 Mrad(SiO_2), at a dose rate of 0.54 krad(SiO_2)/s.

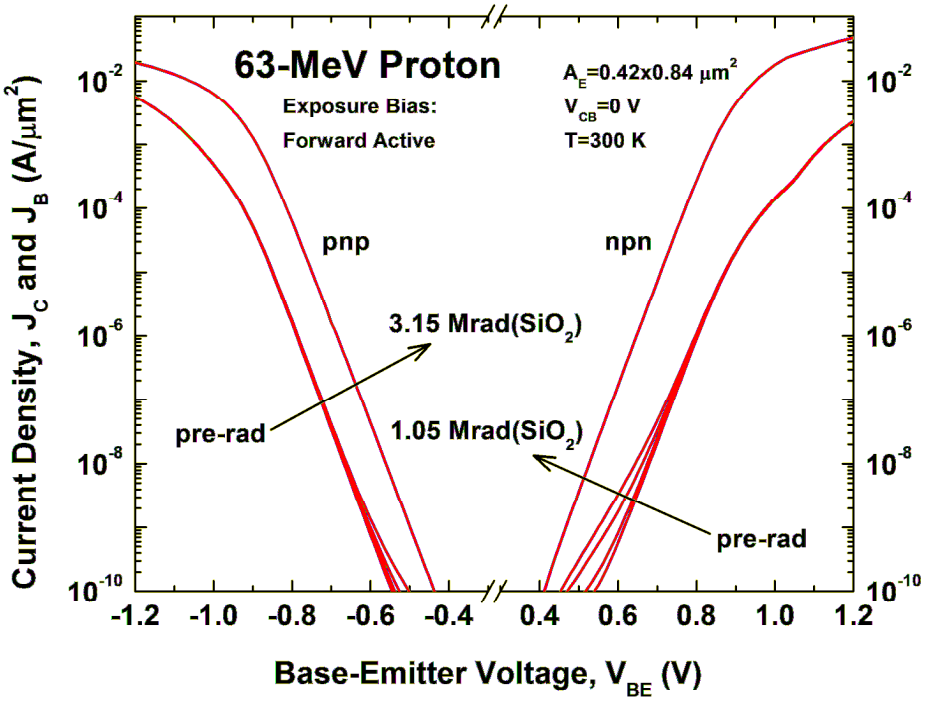

Figure 4: Forward mode *npn* and *pnp* Gummel characteristics from forward-active 63-MeV proton exposure up to 1.05 Mrad(SiO_2) and 3.15 Mrad(SiO_2), at a dose rate of 1.05 krad(SiO_2)/s.

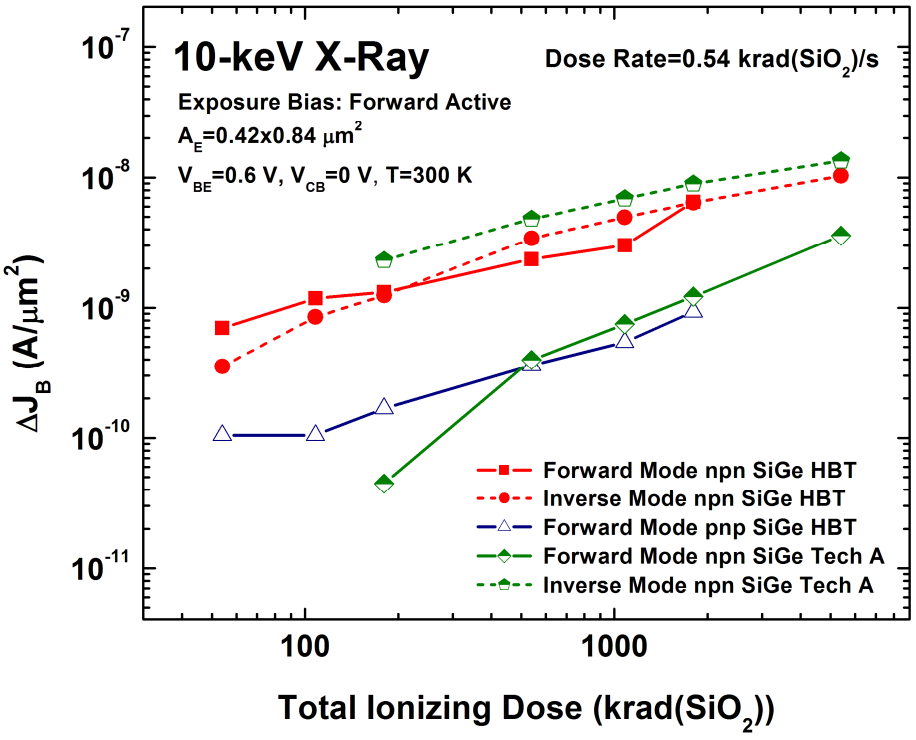

Figure 5: Excess base current, ΔJ_B, plotted as a function of 10-keV X-ray dose for both complementary structures and a comparable *npn*-only 200 GHz technology.

noticeable discrepancy between the excess base current of the irradiated *npn* and *pnp* SiGe HBTs at fixed total dose [16], [4].

The change in base current density across total dose at a fixed V_{BE} of 0.6 V can be seen in Figures 5-7, with Figures 5 and 6 comparing the radiation response of the technology being investigated with previously reported results from a similar 200 GHz *npn*-only technology under X-ray and proton irradiation conditions, respectively [17]. For a device operating in inverse mode, the shallow trench isolation (STI) separating the base from the extrinsic collector is the primary region where damage will induce excess base current [15]. The forward and inverse mode excess base currents for the *npn* devices are comparable, indicating similar contributions from the G/R centers at the EB spacer and STI interfaces. Inverse mode data for the *pnp* devices, however, contained high levels of

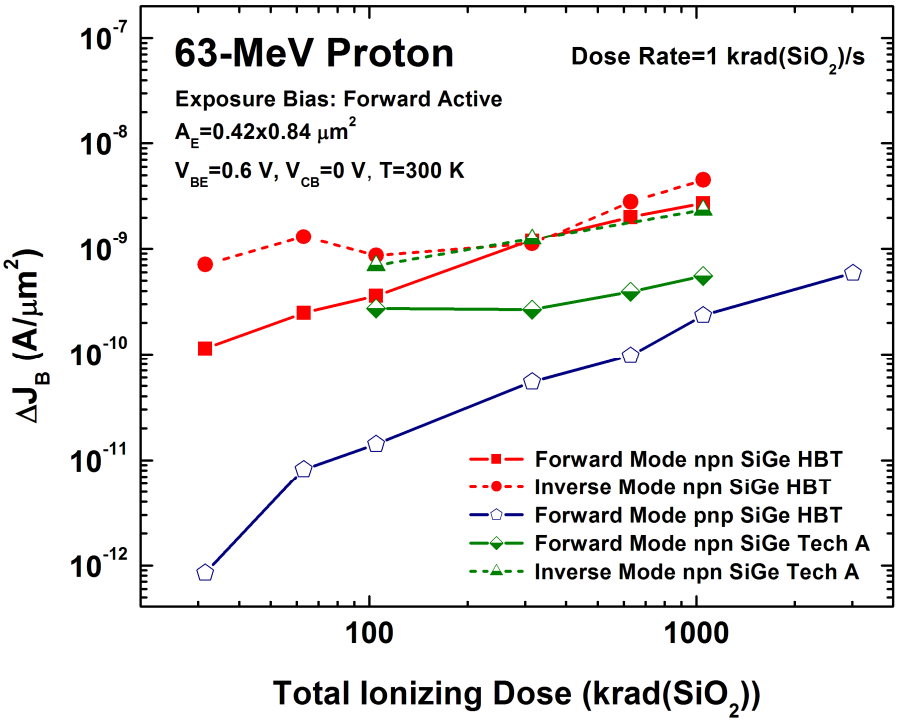

Figure 6: Excess base current, ΔJ_B, plotted as a function of 63-MeV proton dose for both complementary structures and a comparable *npn*-only 200 GHz technology.

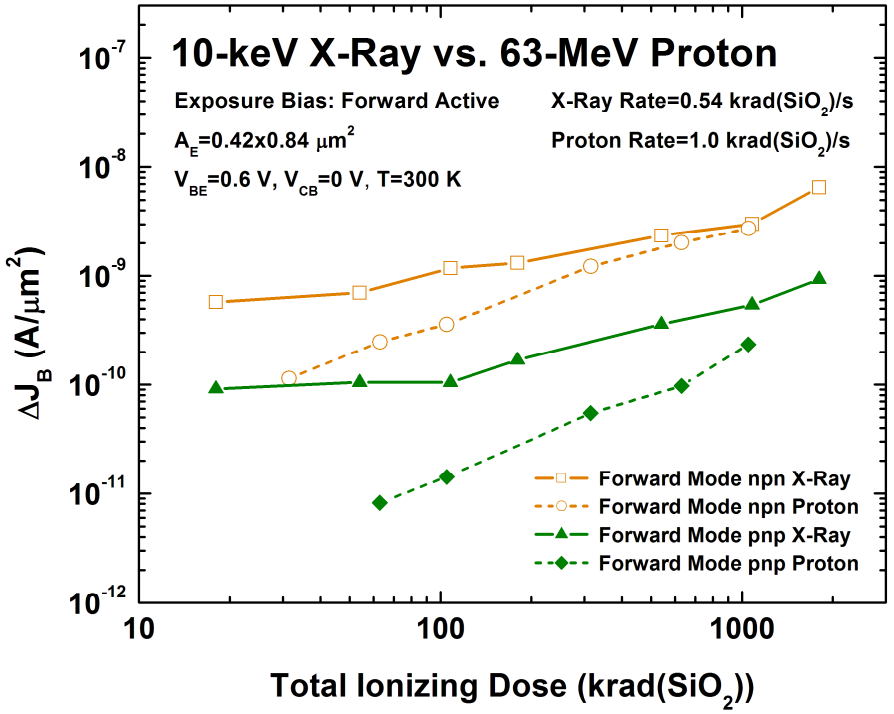

Figure 7: Excess base current, ΔJ_B, plotted as a function of 10-keV X-ray and 63-Mev proton dose for both *npn* and *pnp* structures.

base current at low bias prior to irradiation and are not presented here. The technology under investigation showed slightly more radiation-induced base current from both radiation sources compared with the *npn*-only technology, particularly in forward mode, though neither exhibited substantial damage [4].

Figure 7 offers a direct comparison between X-ray and proton radiation response for the *npn* and *pnp* HBTs. It can be seen that protons produced nearly a decade less excess base current at low dose, with the responses converging as dose increased. Normalized current gain curves are plotted in Figures 8 and 9, illustrating the effects of total dose exposure in a more circuit-relevant context. The gain degradation for the *npn* devices becomes non-negligible only at current densities more than two decades above that of the *pnp*, which remains nearly unaffected by ionizing radiation above current densities of 1.0 $\mu A/\mu m^2$ [4].

AC characterization was performed pre- and post-radiation on custom-designed structures under X-ray total dose exposures up to 1.8 Mrad(SiO_2). The data shown in Figures 10 and 11 are for emitter geometries of 0.63x0.84 μm^2 on all devices except the forward mode *pnp* data, which were obtained from a device with an emitter geometry of 1.26x0.84 μm^2. AC response was similar for all device sizes, showing only slight deviations across total dose that are well within the bounds of measurement error. The collector-base junction bias was held at 0 V for all measurements and the reported data have been normalized to peak f_T for the *npn* devices [4].

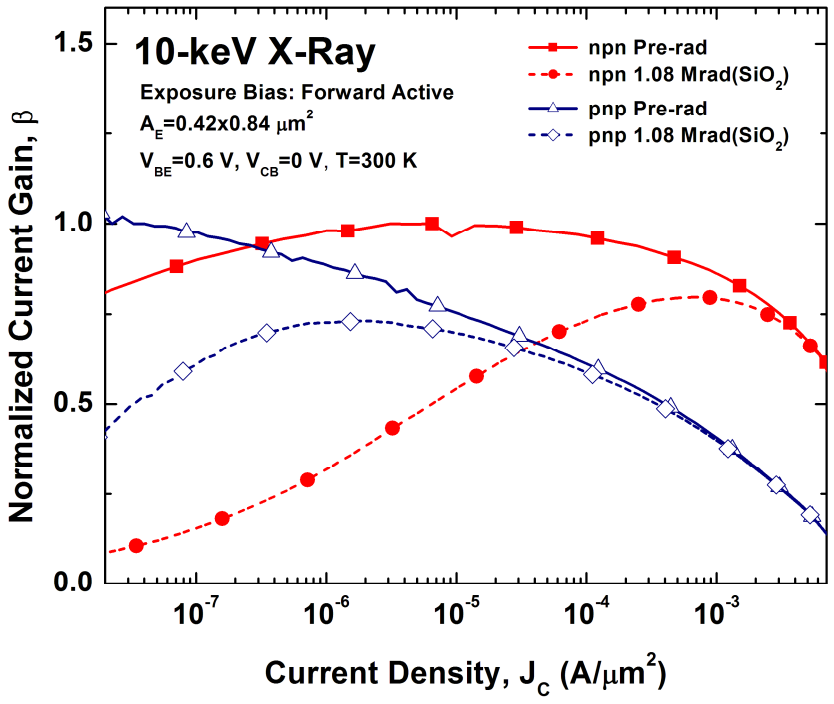

Figure 8: Normalized gain plotted against collector current density for *npn* and *pnp* HBTs before and after 10-keV X-ray exposure at a dose rate of 0.54 krad(SiO_2)/s.

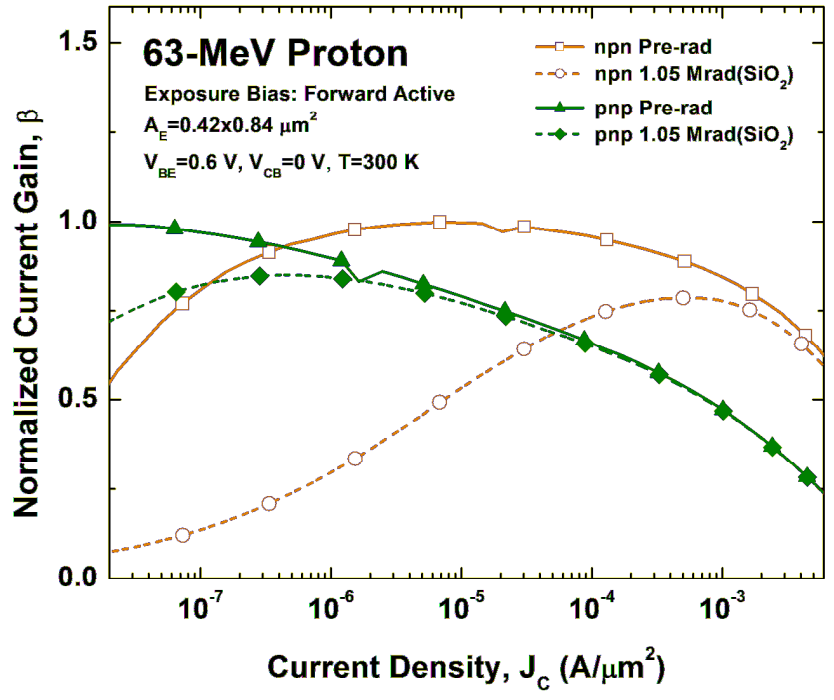

Figure 9: Normalized gain plotted against collector current density for *npn* and *pnp* HBTs before and after proton 63-MeV proton exposure at a dose rate of 1.05 krad(SiO_2)/s.

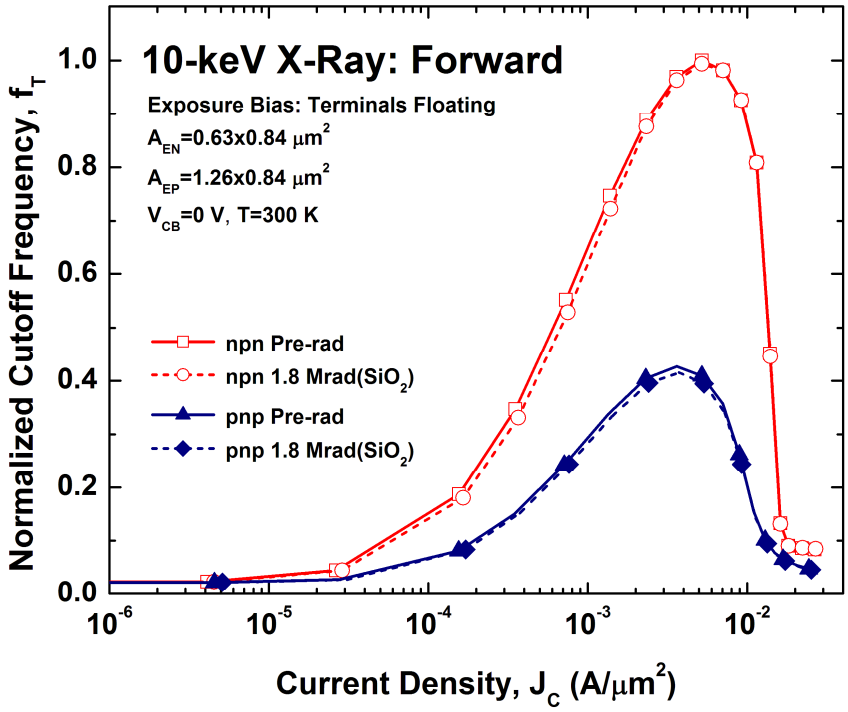

Figure 10: Forward mode unity gain cutoff frequency plotted against collector current density for *npn* and *pnp* SiGe HBTs before and after X-ray exposure.

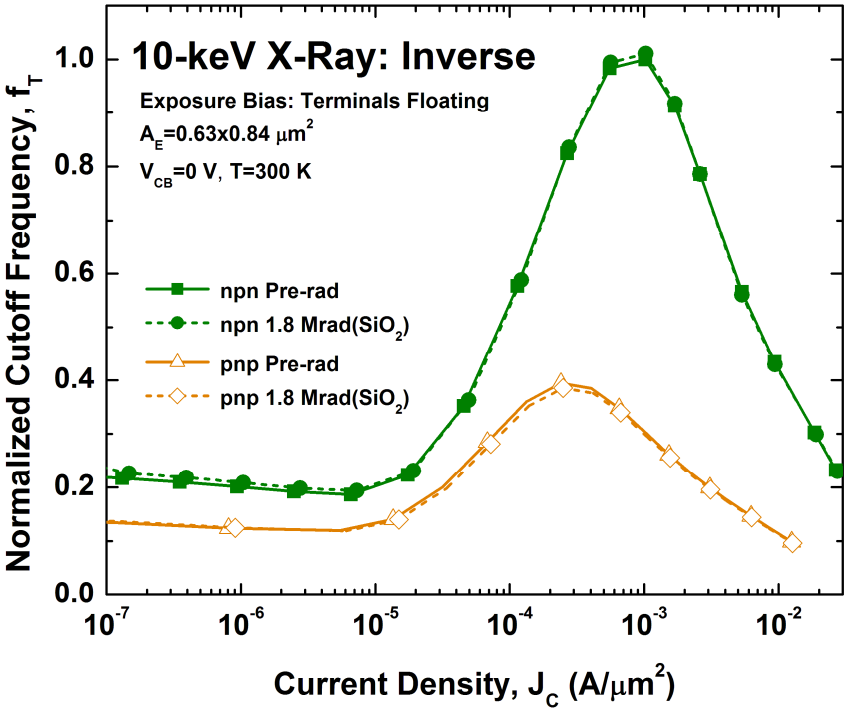

Figure 11: Inverse mode unity gain cutoff frequency plotted against collector current density for *npn* and *pnp* SiGe HBTs before and after x-ray exposure.

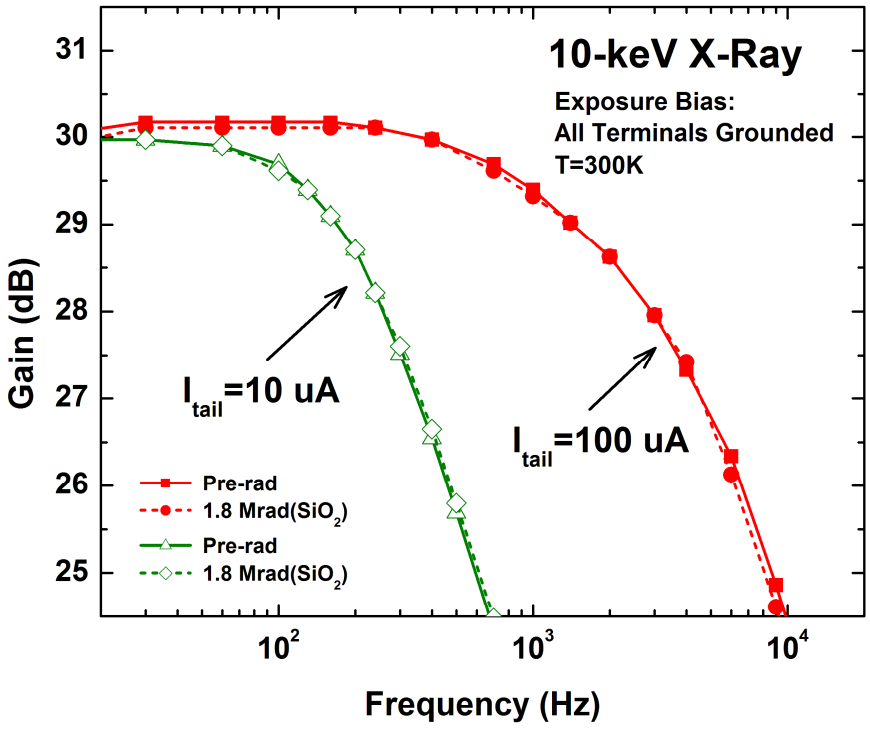

Figure 12: Gain plotted against frequency before and after X-ray irradiation for two low current density bias conditions. Collector current densities are 570 μA/μm^2 and 57 μA/μm^2, respectively.

Pre- and post-irradiation measurements were made on the current feedback operational amplifier in a unity gain configuration with 1.0 mA bias current. The amplifier showed no degradation in performance metrics up to a dose of 1.8 Mrad(SiO_2). In order to probe the effects of the radiation damage at lower current densities, a second experiment was performed. This time the amplifier was configured in a finite gain mode (roughly 30 dB) with tail currents of 100 μA and 10 μA, and was again irradiated to a total dose of 1.8 Mrad(SiO_2). Figure 12 shows the pre- and post-radiation gain curves for both bias conditions. It is readily apparent that despite being biased in a manner that would induce noticeable *npn* gain reduction (25% at $J_C \approx 60$ μA/μm^2) in the individual active devices, the amplifier suffers no ill effects as a result of radiation exposure. The f_{-3dB} remains

constant at 400 Hz and 5 kHz for bias currents of 10 μA and100 μA, respectively, with no low frequency gain degradation in either case [4].

2.4 TID Discussion

The results of the comparison between *npn* and *pnp* devices indicate that the *pnp* SiGe HBTs tend to suffer less damage than their *npn* counterparts, all else being equal. As reported in [18], this can be attributed to the fact that the introduction of radiation-induced positive oxide charge in a *pnp* transistor will accumulate the n-type base region close to the EB spacer, and because recombination occurs more readily when the electron and hole densities are approximately equal, effectively reduce the rate of recombination at that location. This is in contrast to the p-type base region of an *npn* device, which tends to deplete in the presence of positive oxide charge. Assuming a similar contribution to excess base current due to traps at the Si-SiO_2 interface of the EB spacer, this difference could potentially account for the higher total dose tolerance of *pnp* SiGe HBTs [4].

In the circuit context investigated, the amplifier's closed-loop gain and bandwidth are maintained despite reduction in gain for the active devices at low bias currents. This can be at least partially explained by specific characteristics of the circuit topology itself. The gain stage of the current-feedback amplifier consists of two Wilson current mirrors, which together mirror the currents through the inverting input node, pushing them into a high-impedance output and providing voltage gain. A simplified Wilson current mirror is shown schematically in Figure 13. Typical bipolar cascode current mirrors, while providing high output impedance, suffer from the effects of systematic gain error stemming from the finite β_F of the bipolar transistor [19], [4]. When $\beta_F >> 1$,

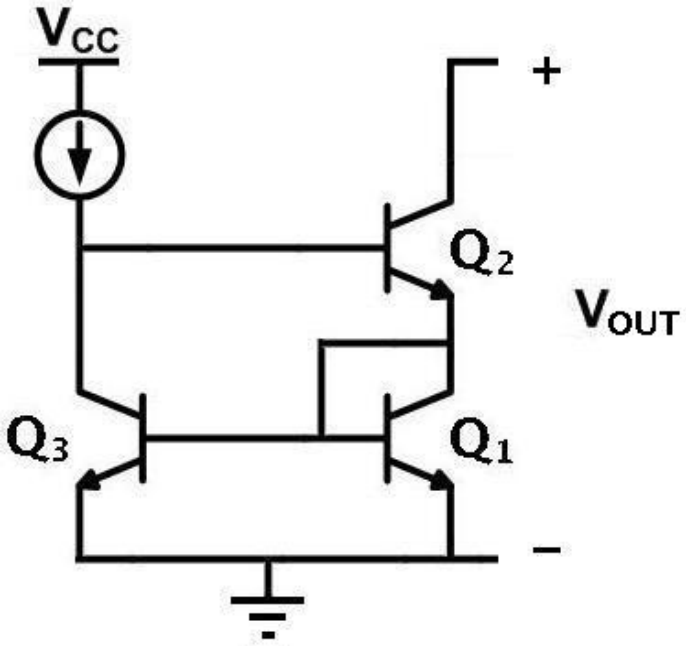

Figure 13: Simplified schematic of the *npn* Wilson current mirror.

$$\varepsilon_{cascode} = -\frac{4}{\beta_F + 4} \tag{1}$$

Changes in β_F, as are induced by radiation damage, for instance, will directly alter the gain error of such stages. The Wilson current mirror mitigates this drawback by providing a feedback path. The current that enters the base of Q_2 produces an emitter current equal to $I_{B2}(\beta_F + 1)$. This current is then mirrored back to Q_3 through Q_1, maintaining I_{C2} such that it is nearly equal to the input current, resulting in less dependence on any changes in β_F. The systematic gain error of the Wilson current mirror due to finite current gain is calculated as [19], [4],

$$\varepsilon_{Wilson} = -\frac{2}{\beta_F^2 + 2\beta_F + 2} \tag{2}$$

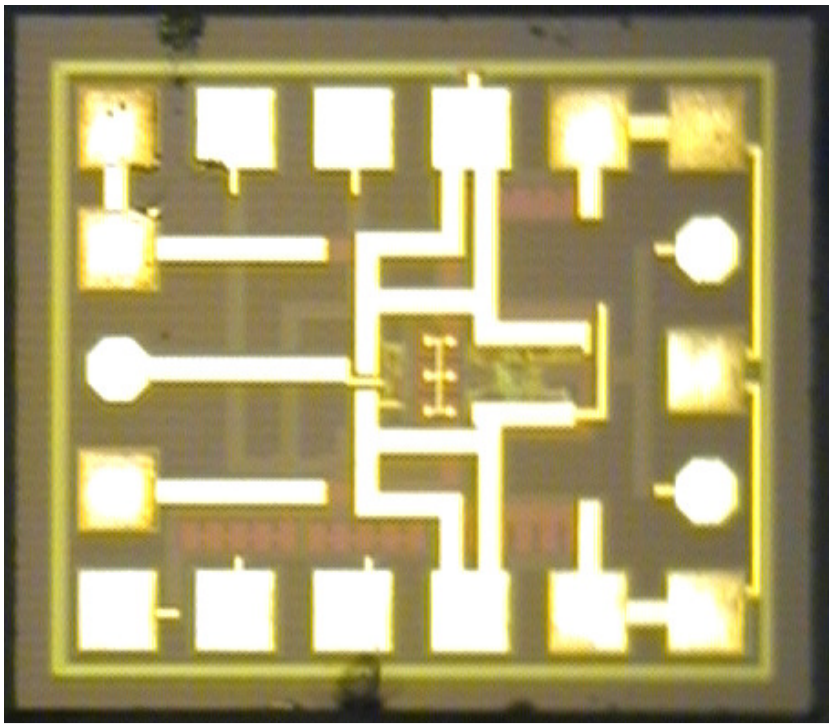

Figure 14. Die photo of the current-feedback operational amplifier.

The gain of the Wilson current mirror also depends on its output impedance, which is directly proportional to β_0 and is calculated approximately as,

$$R_o \approx \frac{\beta_0 r_{o2}}{2} \tag{3}$$

For the current-feedback amplifier, however, the output impedance of the gain stage is in fact the parallel combination of an *npn* and a *pnp* Wilson current mirror. Assuming that r_o and β_0 are both smaller for the *pnp* (whose β_0 does not change significantly at such bias conditions due to irradiation), the output impedance, and therefore the gain, will remain relatively constant for any changes induced in $\beta_{0,npn}$. These trends are consistent with our measured post-irradiation data. A die photo of the current feedback operational amplifier is shown in Figure 14 [4].

CHAPTER III

SINGLE EVENT HARDENING

3.1 Junction Isolated Design

The implementation of junction isolation in the IHP design kit required very few violations of standard design rules. The standard HBT cell already included a p-well substrate contact ring surrounding the STI of the device. All that was necessary was to add a diode junction surrounding that p-well. The design layer chosen was an n-type implant that extends deeper than the subcollector implant used in the HBTs structure. Multiple variants were constructed to determine how aggressively spaced the ring could be from the intrinsic device before electrical malfunctions such as punch-through were detected.

Figures 15 and 16 show schematic cross-sections for the unhardened and junction isolation hardened SiGe HBTs, respectively. The junction-isolated structures shown in Figure 2 were comprised of three variants, with junction widths ranging from 2.2 μm to 2.9 μm. For reference, both Figures 15 and 16 include dotted lines indicating where DTI would normally be present in a comparable 3rd generation technology. Figure 3 shows top-down schematic views of the unhardened and junction isolation hardened HBTs. Implementing the junction isolation increases the area of the HBT from roughly 54 μm^2 to 155 μm^2 [20].

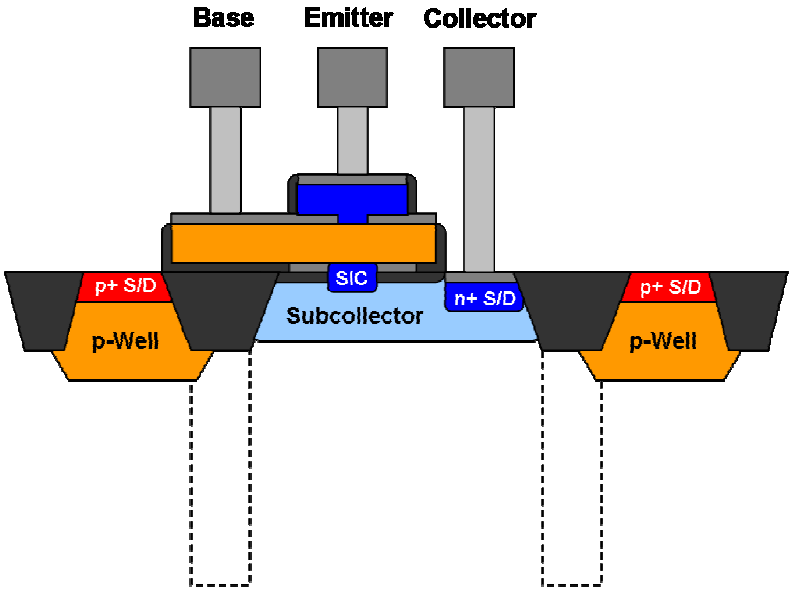

Figure 15: Schematic cross-section of the basic *npn* SiGe HBT. The location of typical deep trench isolation in comparable SiGe technologies is represented by the dotted lines.

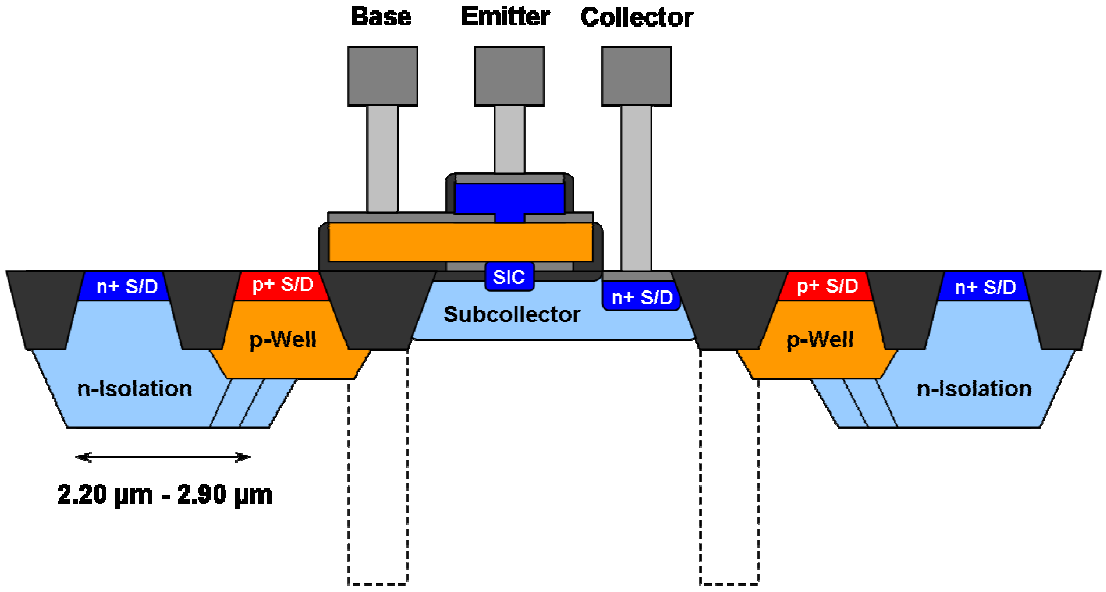

Figure 16: Schematic cross-section of the hardened *npn* SiGe HBT structure showing junction-isolation RHBD variants from 2.2 µm to 2.9 µm wide. The location of typical deep-trench isolation in comparable SiGe technologies is represented by the dotted lines.

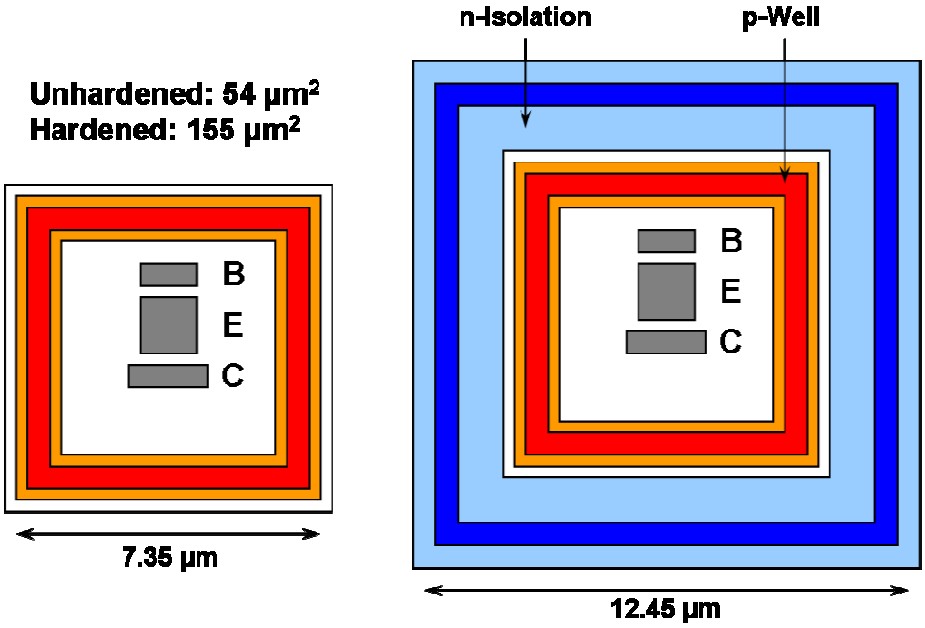

Figure 17: Top-down schematic view of the unhardened (left) and hardened (right) SiGe HBT structure. The junction isolation is shown in blue.

3.2 Test Conditions and Facilities

To determine the effectiveness of the junction isolation RHBD approach, Ion Beam Induced Charge Collection (IBICC) measurements were performed at Sandia National Laboratories, New Mexico with a 36-MeV normal-incidence 16O ion (LET of 7 MeV-cm^2/mg). Charge collection was measured simultaneously on all four terminals connected to amplifier chains composed of Ortec 142A charge sensitive amplifiers and Ortec 671 spectroscopy amplifiers. The testing methodology used is described in detail in [21]. The base, emitter, and substrate terminals of each device were grounded while the collector and n-implant (for RHBD devices) were biased at 3.0 V to emulate realistic circuit operating conditions. To assess total ionizing dose performance, 63 MeV proton irradiation was performed at Crocker Nuclear Laboratory, University of California at

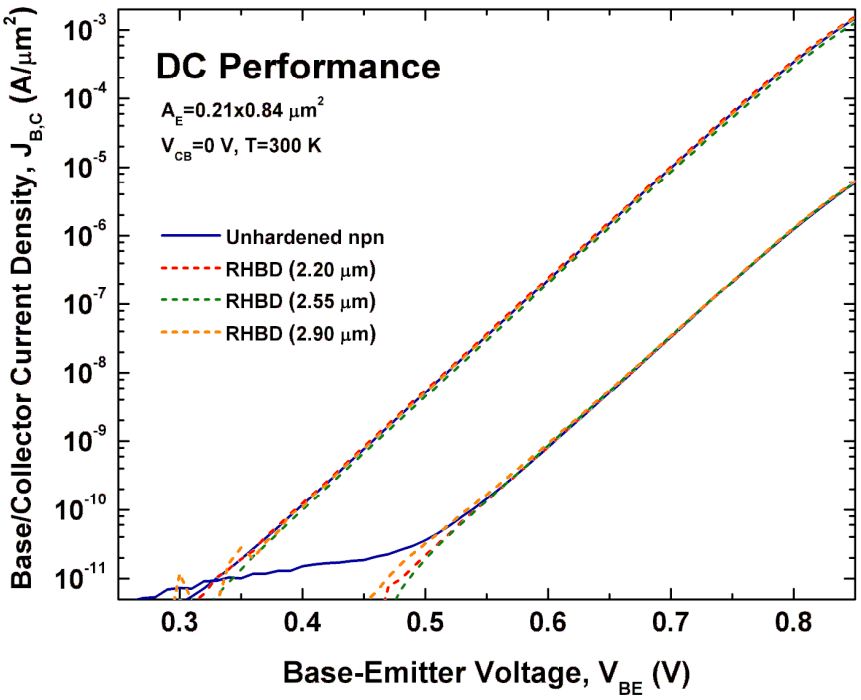

Figure 18: Forward mode Gummel characteristics for the unhardened *npn* SiGe HBT as well as three variants of RHBD devices.

Davis, using a dose rate of 1 krad(SiO_2)/s. All terminals were grounded during exposure and were measured at room temperature in incremental dose steps up to 1.05 Mrad. For both experiments the SiGe HBTs were wire-bonded into 28-pin DIP packages [20].

3.3 Single Event Radiation Results

Initial tests on the junction-isolated structures were aimed at determining whether the presence of the RHBD had any negative effect on basic device performance metrics. Figure 18 shows forward Gummel characteristics for three RHBD variants, as well as the control (unhardened) structure (A_E = 0.21x0.84 μm^2). No significant differences in DC performance were seen for any of the four tested variants. The n-implant was biased at

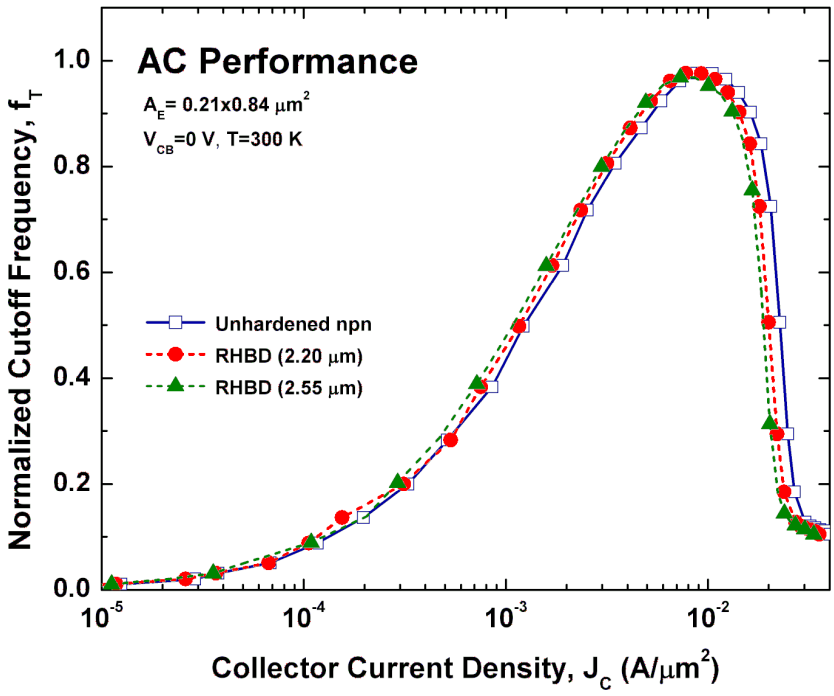

Figure 19: Normalized cutoff frequency plotted against collector current density for the unhardened *npn* SiGe HBT as well as two variants of n-ring hardened devices.

3.0 V during all measurements for consistency. As shown in Figure 19, which plots normalized unity-gain cutoff frequency against collector current density for the control, the 2.2 μm RHBD device, and the 2.55 μm RHBD device, no impact on *ac* performance was observed. For both the DC and AC measurements, V_{CB} was held at 0 V [20].

Further qualification of the proposed SEE hardening technique required that the TID tolerance of the devices be verified. Figure 20 shows forward Gummel characteristics for the two structures. On the left is a control SiGe HBT irradiated to 1.05 Mrad and showing base current degradation in incremental dose steps. On the right is the 2.2 μm junction-isolated RHBD device, irradiated to a maximum dose of 1 Mrad. The increasing base current with total ionizing dose has been previously documented and is the result of the production of traps near the emitter-base (EB) spacer [15]. Figure 21 plots normalized current gain against collector current density from

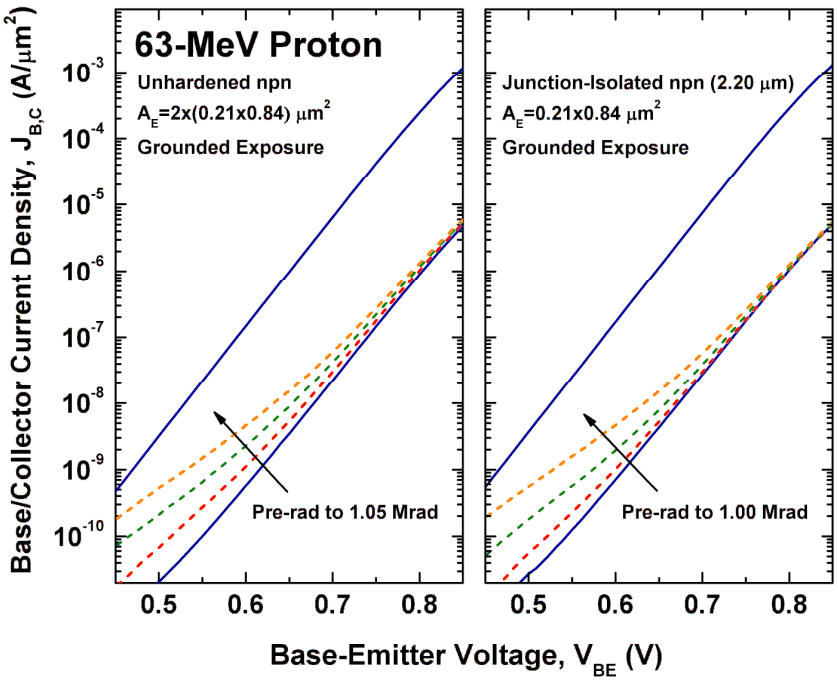

Figure 20: Forward-mode Gummel characteristics for proton irradiated devices with (right) and without (left) junction isolation RHBD.

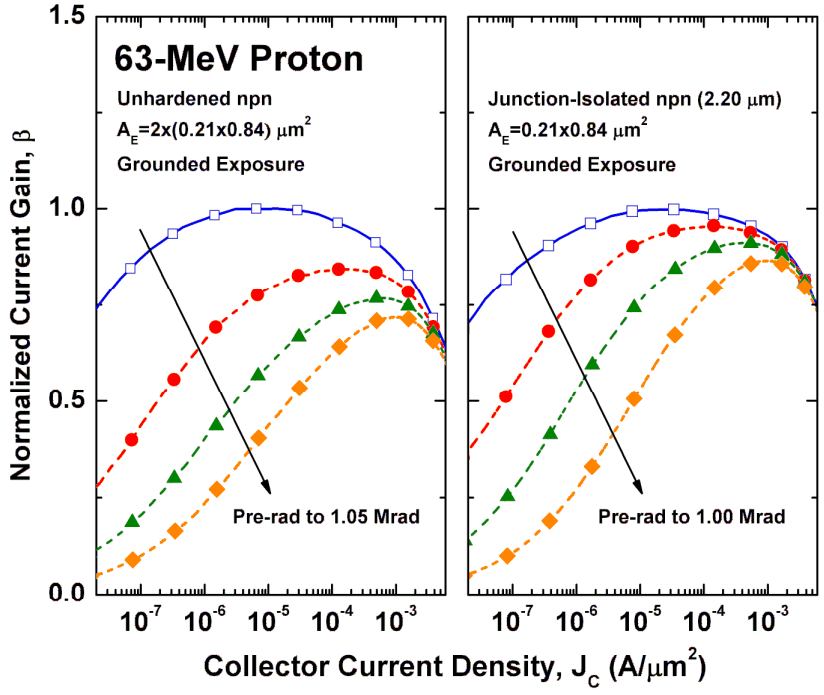

Figure 21: Normalized current gain vs. collector current density for proton irradiated devices with (right) and without (left) RHBD.

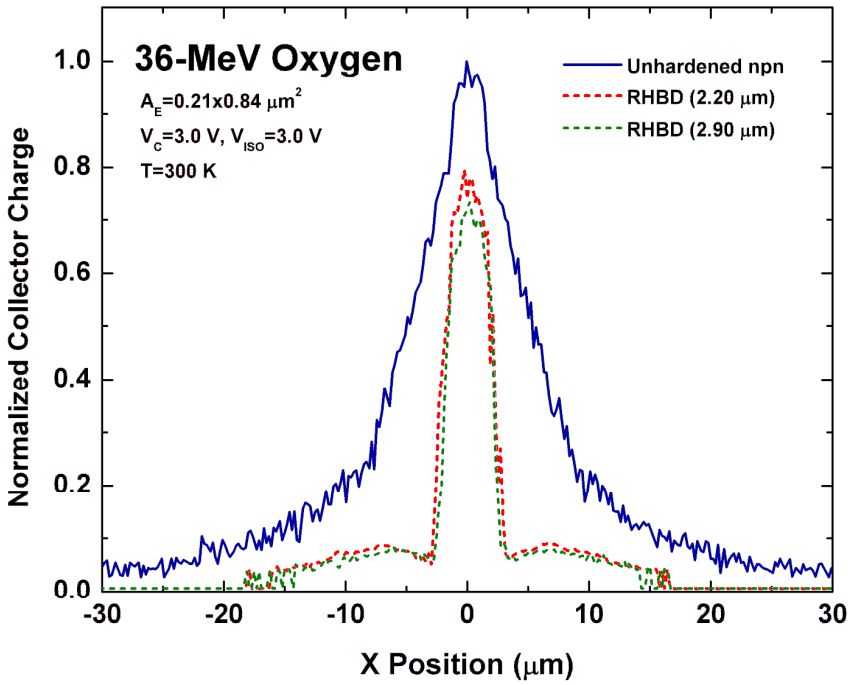

Figure 22: Charge collection in the subcollector during oxygen microbeam irradiation for both the unhardened *npn* SiGe HBT and two RHBD variants.

the same datasets. As in the previous figure, the control results are shown on the left, while the 2.2 μm RHBD device results are shown on the right. The gain degradation curves are almost indistinguishable, indicating as expected that the addition of the junction isolation has no effect on the TID tolerance of the device [20].

To determine whether the junction isolation RHBD would fulfill its intended purpose, IBICC testing was performed on all device variants and the control. Figure 22 illustrates the substantial reduction in charge collection afforded by this new hardening technique. The curves represent a 2 μm wide slice in the x-direction through the center of the device, while the contours in Figures 23 and 24 represent the entire surface. Each dataset consists of numerous scans of the area containing the DUT, and for each x-y location, only the maximum collected charge is plotted (subtracting outliers). Clearly the pn-junction

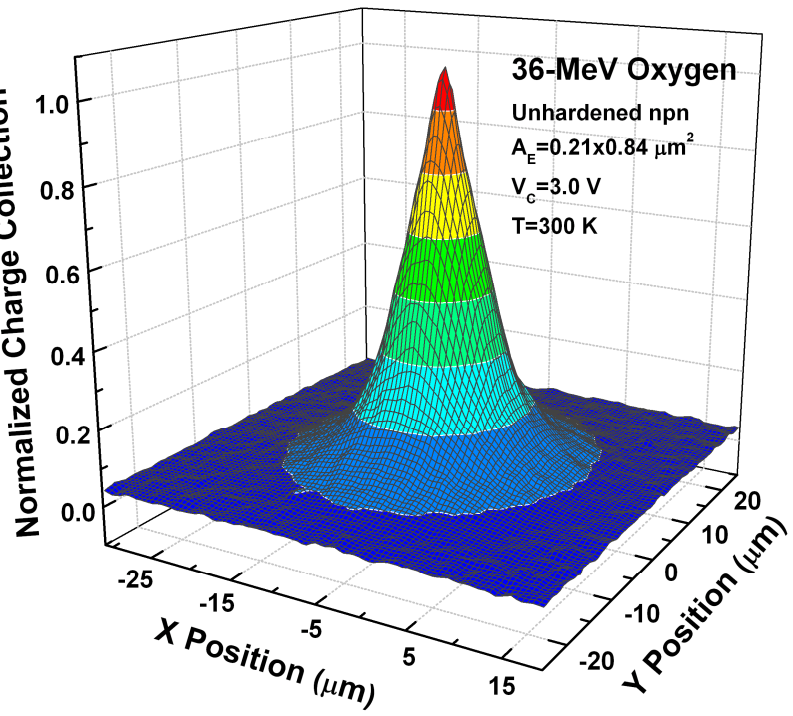

Figure 23: Normalized collected charge for the unhardened *npn* SiGe HBT as a function of strike location.

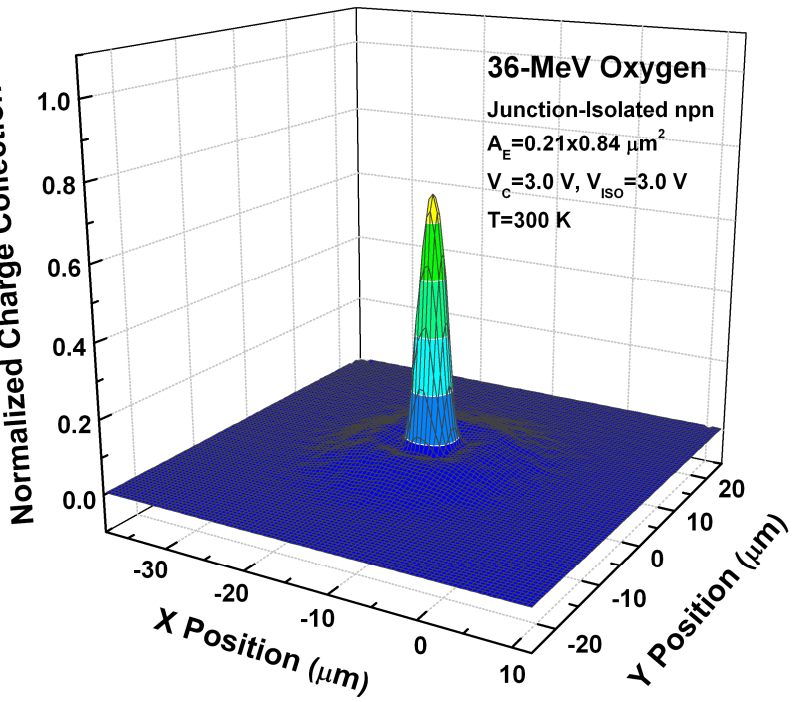

Figure 24: Normalized collected charge (to the peak of Figure 23) for the RHBD *npn* SiGe HBT as a function strike location.

isolation in the hardened devices, starting at roughly ±4 µm, absorbs a substantial amount of charge for strikes in its vicinity. Observe as well the 25% reduction in charge collection for center emitter strikes, peaking at only 128 fC for the most conservative hardening scheme [20].

The two hardened variants exhibited only small differences, with the more aggressive 2.9 µm n-ring design achieving a slightly better charge collection profile. Figure 25 plots the same charge collection data integrated over the x-axis. The RHBD SiGe devices showed nearly a 70% reduction in integrated charge collection over the control device. Figure 26 shows the best achieved results using more traditional third-generation n-ring RHBD outside of the DTI (e.g., in IBM SiGe 8HP) [8]. The present results represent the most effective transistor layout-level RHBD demonstrated to date in SiGe. While there is an incurred device area penalty for SEU mitigation incurred by the present RHBD approach, as shown in Figure 17, this should have minimal impact for actual circuit design complexity or net circuit real estate, given that SiGe circuits are typically not transistor-area limited [20].

3.4 SEE Discussion

This investigation shows that device-level SEU hardening of most 3rd generation SiGe HBT technologies can be hindered by the presence of deep trench isolation. By the addition of a simple yet effective junction isolation RHDB scheme into a SiGe process without DTI, we have developed an effective hardening technique capable of helping mitigate both outside DTI strikes and inside DTI strikes. The junction isolation RHBD was able to reduce the peak collected charge from a center striking 36-MeV oxygen ion

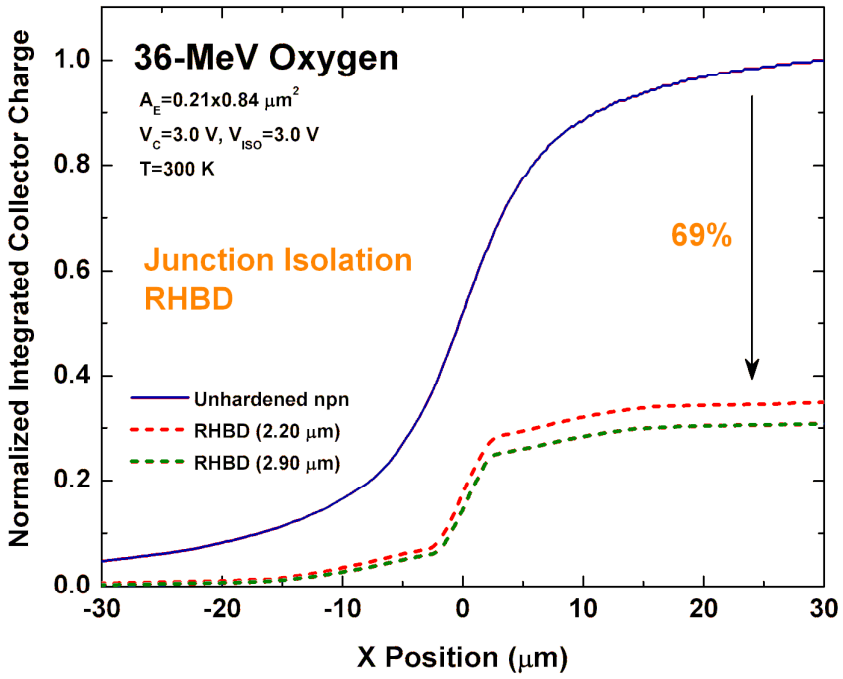

Figure 25: Integrated charge across ion strike location for both the unhardened *npn* SiGe HBT and two RHBD variants with shallow trench isolation.

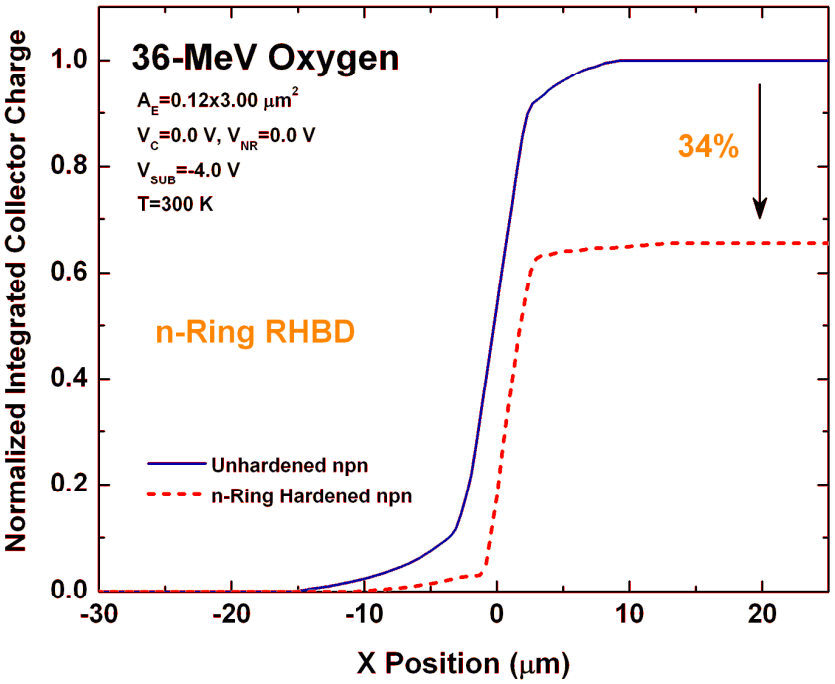

Figure 26: Integrated charge across ion strike location for both unhardened and n-ring hardened 8HP SiGe HBTs with deep trench isolation.

to a mere 128 fC, and achieve the most effective device-level reduction of total integrated charge in a SiGe HBT to date. These advantages are obtained at no penalty to other performance metrics, with no process modification, and with only a modest area penalty [20].

3.5 Future Work

Further qualification of the effectiveness of junction isolation will require circuit level assessment of saturated cross-section and upset thresholds under broad-beam, heavy ion radiation. Common-mode logic shift registers with and without junction isolation would provide excellent comparison of the saturated cross section if measured with a Bit Error Rate Tester (BERT) during exposure. In addition, TCAD modeling of the device structure with and without hardening would provide valuable insight into the behavior of the electric fields and free charge beneath the subcollector in the event of a strike. Together with the present work, these would provide a much more complete picture of the viability of junction isolation RHBD for space-based applications.

CHAPTER IV

CONCLUSION

This work has tested and verified the total-dose radiation tolerance of a third generation complementary SiGe:C BiCMOS technology platform. DC and AC characterization showed both the *npn* and *pnp* to be resilient to x-ray and proton radiation doses as high as 1 Mrad. Further investigation of an *npn* / *pnp* only current feedback operational amplifier supported these findings, showing no appreciable degradation of performance metrics. These results can be partly attributed to the design of the amplifier, which utilized Wilson current mirrors to reduce gain error [4].

To bolster the radiation tolerance of an HBT technology, particularly for mixed-signal applications, the inherent sensitivity to single event phenomena must be addressed at the process, device, or circuit level. A novel device-level approach known as junction isolation RHBD has been proposed and tested, showing very promising results under microbeam radiation. The technique, consisting of an n-type junction surrounding the device, depends on the absence of deep trench isolation to allow for improved charge collection in the event of center-emitter strikes. The results presented here show a reduction of integrated charge collection across the device of 69%, representing the most effective device level hardening in a SiGe HBT to date [20].

REFERENCES

[1] CRESSLER, J.D., "On the Potential of SiGe HBTs for Extreme Environment Electronics," *Proceedings of the IEEE*, vol. 93, no. 9, pp. 1559-1582, September 2005.

[2] SUTTON, A.K., *et al.*, "A Comparison of Gamma and Proton Radiation Effects in 200 GHz SiGe HBTs," *IEEE Transactions on Nuclear Science*, vol. 52, no. 6, pp. 2358-2365, December 2005.

[3] SUTTON, A.K., *et al.*, "Proton Tolerance of Fourth-generation 350 GHz UHV/CVD SiGe HBTs," *IEEE Transactions on Nuclear Science*, vol. 51, no. 6, pp. 3736-3742, December 2004.

[4] DIESTELHORST, R.M., *et al.*, "The Effects of X-ray and Proton Irradiation on a 200 GHz / 90 GHz Complementary (*npn* + *pnp*) SiGe:C HBT Technology," *IEEE Transactions on Nuclear Science*, vol. 54, no. 6, pp. 2190-2195, December 2007.

[5] CRESSLER, J.D., *et al.*, *Silicon-Germanium Heterojunction Bipolar Transistors*. Boston: Artech House, 2003.

[6] CRESSLER, J.D., *et al.*, "A High-speed Complementary Silicon Bipolar Technology with 12-fJ Power-delay Product," *IEEE Electron Device Letters*, vol. 14, no. 11, pp. 523-526, November 1993.

[7] REED, R.A., *et al.*, "Heavy-ion Broad-beam and Microprobe Studies of Single-event Upsets in 0.20-µm SiGe Heterojunction Bipolar Transistors and Circuits," *IEEE Transactions on Nuclear Science*, vol. 50, no. 6, pp. 2184-2190, December 2003.

[8] SUTTON, A.K., *et al.*, "An Evaluation of Transistor-layout RHBD Techniques for SEE Mitigation in SiGe HBTs," *IEEE Transactions on Nuclear Science*, vol. 54, no. 6, pp. 2044-2052, December 2007.

[9] HEINEMANN, B., *et al.*, "A Complementary BiCMOS Technology with High Speed npn and pnp SiGe:C HBTs," *IEDM Technical Digest*, pp. 117-120, December 2003.

[10] HEINEMANN, B., C., *et al.*, "Novel Collector Design for High-speed SiGe:C HBTs," *IEDM Technical Digest*, pp. 775-778, December 2002.

[11] MURRAY, K.M., STAPOR, W.J., CASTENEDA, *et al.*, "Calibrated charged particle radiation system with precision dosimetric measurement and control," *Nuclear Instruments and Methods in Physics Research Section A*, vol. 281, pp. 616-621, September 1989.

[12] ALLEN, P.E., TERRY, M.B., "The Use of Current Amplifiers for High Performance Voltage Applications," *IEEE Journal of Solid-State Circuits*, vol. SC-15, no. 2, pp. 155-162, April 1980.

[13] "Current Feedback Amplifiers," *National Semiconductor Corporation Application Note OA-31*, Nov. 1992.

[14] BALES, J., "A Low-power, High-speed, Current-feedback Op-amp with a Novel Class AB High Current Output Stage," *IEEE Journal of Solid-State Circuits*, vol. 32, no. 9, pp. 1470-1474, September 1997.

[15] CRESSLER, J.D., *et al.*, "An Investigation of the Origins of the Variable Proton Tolerance in Multiple SiGe HBT BiCMOS Technology Generations," *IEEE Transactions on Nuclear Science*, vol. 49, no. 6, pp. 3203-3207, December 2002.

[16] ZHAO, E., *et al.*, "The Effects of Radiation on 1/f Noise in Complementary (*npn* + *pnp*) HBTs," *IEEE Transactions on Nuclear Science*, vol. 51, no. 6, pp. 3243-3249, December 2004.

[17] SUTTON, A.K., *et al.*, "An Investigation of Dose Rate and Source Dependent Effects in 200 GHz SiGe HBTs," *IEEE Transactions on Nuclear Science*, vol. 53, no. 6, pp. 3166-3174, December 2006.

[18] SCHMIDT, D.M., *et al.*, "Comparison of Ionizing-radiation-induced Gain Degradation in Lateral, Substrate, and Vertical pnp BJTs," *IEEE Transactions on Nuclear Science*, vol. 42, no. 6, pp. 1541-1549, December 1995.

[19] GRAY, P.R., *et al.*, *Analysis and Design of Analog Integrated Circuits*, Fourth Edition. New York: Wiley, 2001.

[20] DIESTELHORST, R.M., *et al.*, "Junction Isolation Single Event Radiation Hardening of a 200 GHz SiGe:C HBT Technology Without Deep Trench Isolation," *IEEE Transactions on Nuclear Science*, December 2009.

[21] REED, R.A. *et al.*, "Heavy-ion Broad-beam and Microprobe Studies of Single-event Upsets in a 0.20-μm SiGe Heterojunction Bipolar Transistors and Circuits," *IEEE Transactions on Nuclear Science*, vol. 50, no. 6, pp. 2184–2190, December 2003.